# QM/MM Protocol for Direct Molecular Dynamics of Chemical Reactions in Solution: The Water-Accelerated Diels−Alder Reaction

Zhongyue Yang,[†] Charles Doubleday,*[,‡] and K. N. Houk*[,†]

[†]Department of Chemistry and Biochemistry, University of California, Los Angeles, California 90095, United States
[‡]Department of Chemistry, Columbia University, 3000 Broadway, MC 3142, New York, New York 10027, United States

S *Supporting Information*

ABSTRACT: We describe a solvent-perturbed transition state (SPTS) sampling scheme for simulating chemical reaction dynamics in condensed phase. The method, adapted from Truhlar and Gao's ensemble-averaged variational transition state theory, includes the effect of instantaneous solvent configuration on the potential energy surface of the reacting system (RS) and allows initial conditions for the RS to be sampled quasiclassically by TS normal mode sampling. We use a QM/MM model with direct dynamics, in which QM forces

of the RS are computed at each trajectory point. The SPTS scheme is applied to the acceleration of the Diels−Alder reaction of cyclopentadiene (CP) + methyl vinyl ketone (MVK) in water. We explored the effect of the number of SPTS and of solvent box size on the distribution of bond lengths in the TS. Statistical sampling of the sampling was achieved when distribution of forming bond lengths converged. We describe the region enclosing the partial bond lengths as the transition zone. Transition zones in the gas phase, SMD implicit solvent, QM/MM, and QM/MM+QM (3 water molecules treated by QM) vary according to the ability of the medium to stabilize zwitterionic structures. Mean time gaps between formation of C−C bonds vary from 11 fs for gas phase to 25 fs for QM/MM+QM. Mean H-bond lengths to O(carbonyl) in QM/MM+QM are 0.14 Å smaller at the TS than in MVK reactant, and the mean O(carbonyl)−H(water)−O(water) angle of H-bonds at the TS is 10° larger than in MVK reactant.
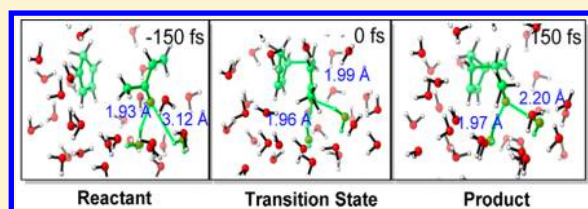
INTRODUCTION

An increasing number of studies point to the importance of nonstatistical dynamics in organic reactions.[1−25] Experimental rate or product ratios in these reactions are poorly described by statistical theories (transition state theory or RRKM theory) but can be understood in terms of nonstatistical dynamical effects revealed by classical trajectory calculations. One area of concern is that most reactions are carried out in solution, but most trajectory calculations either have been applied to gas-phase reactions or have used a dynamical model without explicit solvent for reactions that occur in solution. In this paper, we describe and test a method that could be used to examine short-time nonstatistical dynamics in solution with explicit solvent. The emphasis on short simulation times, typically <500 fs, is useful for minimizing the nonphysical flow of zero point energy (ZPE) within the reacting system. In addition, nonstatistical effects tend to be largest at short times.

In recent years, trajectory calculations (or molecular dynamics, MD) for reactions involving covalent bonding changes in condensed phase have been reported with explicit solvation.[26] These pioneering calculations are a significant advance over gas-phase models. For our purposes, there are specific features that would be useful. The method should (1) sample initial conditions in a way that includes the effect of instantaneous solvent configuration on the potential energy surface of the reacting system and (2) allow initial conditions for the reacting system to be sampled quasiclassically, the method typically used to study nonstatistical dynamics. In

quasiclassical thermal sampling, each vibrational normal mode is given at least the ZPE, and any additional energy is quantized to mimic a quantum Boltzmann distribution of vibrational levels. The proposed method satisfies these requirements.

We use a QM/MM model (quantum mechanics for the reacting system, molecular mechanics for solvent) with direct-dynamics trajectories, in which QM forces are computed at each MD point. The calculation is run within AMBER,[27] which has an interface to Gaussian 09[28] that supports electronic embedding (i.e., allows the electron density of QM solute to be polarized by the MM solvent). AMBER handles the MD part of the calculation (creation of solvent box, equilibration, and propagation of trajectories). The method for sampling initial coordinates and momenta for the QM reacting system is adapted from Truhlar and Gao's ensemble-averaged variational transition state theory, EA-VTST,[29] coupled with transition state (TS) normal mode sampling,[30] a method for quasiclassical sampling of the TS dividing surface used in gas-phase simulations. EA-VTST, which has been extensively applied to enzyme reactions,[29,31] was developed to include vibrational contributions of the reacting system to free energies of activation in condensed phase, and to compute quantum mechanical tunneling. It employs a separation of time scales of fast solute vibrations vs slower solvent motions, such that the reacting system maintains a Boltzmann distribution of vibra-
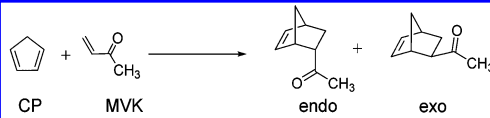
tional levels for any arbitrary configuration of solvent molecules. Our protocol inherits this characteristic.

After describing our model, we apply it to the acceleration of Diels−Alder reactions in water. This reaction is accurately described by statistical theory; it has been well characterized experimentally[32] and computationally[33] and is used here to test statistical convergence in the sampling and to compare the dynamics in several solvent models. The acceleration of Diels−Alder reactions in water was first reported by Breslow,[32] who found that both reactivities and endo/exo selectivities are enhanced by water. Scheme 1 shows Breslow's results for

Scheme 1. Second-Order Rate Constants and Endo/Exo Product Ratios for the CP + MVK Diels−Alder Reaction in Several Solvents[32b]

solvent	$k_2 \times 10^5$ $M^{-1}S^{-1}$(20 °C)	endo/exo ratio
isooctane	5.94±0.3	
methanol	75.5	
water	4400±70	25.0
formamide	318±4	8.9
ethylene glycol	480	10.4

cyclopentadiene (CP) + methyl vinyl ketone (MVK) in several solvents.[32b] The rates span nearly 3 orders of magnitude from isooctane to water. Jorgensen and co-workers[33] have given strong evidence that the largest contribution to the water acceleration of Diels−Alder reactions comes from enhanced hydrogen bonding in the TS vs reactants. In ab initio calculations, they found that larger polarization in the TS than in MVK leads to an increase in H-bond strength at the TS by 1.5−2.0 kcal/mol.[33a] In QM/MM calculations,[33b,c] H-bonding provides a larger free energy contribution in the TS than in reactants or products.

■ COMPUTATIONAL METHODS

M06-2X/6-31G(d) is the QM method used for optimizations and trajectories, and water is represented by the TIP3P[34] MM model. The SMD solvation model of Cramer and Truhlar and co-workers[35] is used in calculations involving implicit solvent.

The full QM/MM system with N atoms consists of a small reacting zone (N_1 reacting atoms treated by QM) and a large solvent zone ($N_2 = N − N_1$ solvent atoms treated by MM). The QM/MM protocol consists of six steps. Further details are in the Supporting Information.

1. The M06-2X/6-31G(d) endo transition structure TS_w is computed with continuum water solvation using SMD.
2. TS_w is surrounded by a cubic solvent box (periodic boundary conditions, electrostatic cutoff is 8 Å), whose size is determined in an iterative method leading to statistical convergence, described below. For a given box size and with TS_w fixed, the solvent is equilibrated for 200 ps in an *NPT* ensemble (fixed number of atoms N, pressure P, and temperature T).[36,37]
3. As solvent equilibration continues with fixed TS_w, a set of instantaneous frozen solvent coordinates and momenta are extracted and stored at 5 ps intervals. This is

continued until a specified number (usually ≤25) of frozen solvent configurations has been picked.

4. For each frozen solvent configuration, the transition structure for the N_1 reacting atoms is optimized using ONIOM,[38] keeping the N_2 solvent atoms fixed. Because each of these solvent-perturbed transition states (SPTSs) is optimized in the field of a different frozen solvent configuration, their geometries and vibrational frequencies differ (shown in Table S1). The number of SPTS saddle points, N_{SPTS}, is equal to the number of frozen solvent configurations in step 3.
5. At each SPTS saddle point, several sets (currently 10) of initial coordinates and momenta for the reacting system are selected quasiclassically by TS normal mode sampling at 300 K. In previous work we have used Venus[39] or Progdyn[9b] for TS normal mode sampling; here we use Progdyn. The bound modes were the $3N_1 − 1$ real frequencies of the reacting system, and the transition vector was the reaction coordinate.[40] This gives initial conditions for $10 \times N_{SPTS}$ trajectories.
6. All constraints on the frozen solvent zone are released, and $10N_{SPTS}$ trajectories for the full system are propagated forward and backward from the initial point until either reactants or products are formed, using velocity Verlet with a 1 fs step size. In the current application, trajectories were stopped after 150 fs in each direction.[41]

To include a QM description of hydrogen bonding during the trajectories, the general procedure above was modified to include two to three water molecules in the QM zone. In step 3, up to three water molecules were identified in each of the N_{SPTS} frozen MM solvent configurations by searching for O−O distances <3 Å between oxygen atoms of water and MVK. Most of these involved H-bonding to the carbonyl oxygen to varying degrees. If only two water molecules were found, a search was made for a third water whose O−O distance to one of the first two waters was <3 Å. In step 4, the chosen water molecules, though frozen, were included in the QM reacting zone during the SPTS optimizations; MM was maintained for the remaining frozen solvent. This allowed the SPTS geometry to be optimized in the presence of frozen QM H-bonds. As a result, the initial coordinates and momenta for CP + MVK determined in step 5 include a QM description of H-bonding to 2−3 frozen waters. Although the QM waters were represented by MM in the equilibration step, the main features of their dynamics should be simulated by this procedure. We refer to this method as QM/MM+QM.

To reach statistical convergence in the sampling, steps 2−5 are repeated with different cubic box sizes in step 2 and different values for N_{SPTS}, the number of frozen solvent configurations in step 3, which is equal to the number of SPTSs in step 4. For each combination of box size and N_{SPTS}, we compute the distribution of forming CC bond lengths in the $10N_{SPTS}$ sampled TS structures. Statistical convergence is achieved at the smallest values of box size and N_{SPTS} at which the distribution stops changing, as illustrated below.

Trajectory calculations were also carried out in the gas phase and with SMD implicit water, for comparison to QM/MM. They were initialized at the saddle point with TS normal mode sampling at 300 K, and propagated 150 fs in forward and reverse directions from the initial point using velocity Verlet with 1 fs step size.

■ RESULTS AND DISCUSSION

Figure 1 shows the H-bonds identified in four solvent configurations after the equilibration with fixed TS_w in step 3.
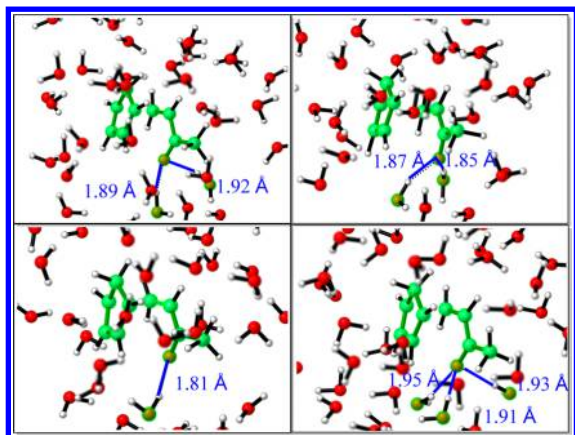

Figure 1. Four solvent configurations after the equilibration with fixed TS_w in step 3. Hydrogen bond lengths are shown (black solid lines).

Two of these configurations have two H-bonds to the carbonyl oxygen, one configuration has one H-bond, and one configuration has three H-bonds. Figure 2a shows the distribution of forming bonds in N_{SPTS} = 20 saddle points produced in step 4. The distribution in Figure 2a illustrates the substantial effect that solvent can exert on the potential energy surface of the reacting system.[29,31] In step 5, each SPTS is sampled to give 10 sets of coordinates and momenta, 200 in all. Figure 2b shows the transition zones, defined as the most probable 98% of the distribution in the forming bond lengths produced by TS normal mode sampling. The 200 sampled TS coordinates are superimposed in the inset.

Figure 3 shows the test for statistical convergence, in which steps 2−5 are carried out with cubic box sizes of 10, 12, and 13 Å (617, 944, and 1137 water molecules, respectively) and N_{SPTS} = 15, 20, 25. This generates nine combinations whose transition zones are shown. As box size and N_{SPTS} are increased, the mean and variance of the transition zones stop changing and convergence is achieved with a 12 Å box and N_{SPTS} = 20.

Figure 4 shows the transition zones for gas phase, SMD implicit solvent, and QM/MM explicit solvent with a 12 Å box and N_{SPTS} = 20. The three QM/MM transition zones include zero, two, and three H-bonded water molecules as described above. The asynchronicity, defined here as the difference

between mean bond lengths in the transition zone, is 0.35 Å in the gas phase and 0.52 Å in SMD. Asynchronicities for QM/MM are close to the SMD value: 0.48, 0.54, 0.54 for 0, 2, and 3 H-bonded waters, respectively. The difference from the gas phase is consistent with zwitterionic stabilization of asynchronous bond formation in water. In Acevedo and Jorgensen's QM/MM study of CP + MVK using PDDG/PM3 as QM in OPLS water, the asynchronicities were 0.1 Å for gas phase and 0.33 in water.[33c]

Figure 5 shows the same set of TS points as in Figure 4, projected onto the plane of C_1C_2 and C_3C_4 distances. From visual inspection it is clear that the QM/MM methods have broader distributions than those for gas phase and SMD. Quantitatively, the standard deviations along the direction of the reaction coordinate (perpendicular to the long axes of the TS distributions) are in the ratio 1:1.2:1.9:2.7 for the gas phase, SMD, QM/MM (no QM H-bonds), and QM/MM+QM (three QM H-bonds), respectively. Inclusion of explicit solvent, and particularly QM H-bonding, is seen to have a substantial effect on the TS distribution.

Table 1 shows the time gaps for bond formation, defined as the difference between the times at which the forming bond lengths first drop below 1.59 Å. Subsequent brief excursions above 1.59 are ignored. TS distributions in Figures 4 and 5 evolve into distributions of time gaps that qualitatively reflect the TS asynchronicities. Both the TS and the species produced by formation of the first bond have zwitterionic character[42] and are stabilized in water. The mean time gap is larger for the three aqueous models than for the gas phase and is largest for QM/MM+QM, which also has the largest TS asynchronicity of the four methods in Table 1.

The time gap distributions are broad with tails extending above 80 fs for the aqueous models including SMD. The percent of time gaps above 35 fs gives an indication of the fraction of trajectories that persist for one or more C−C vibrational periods after forming the first bond. A related measure is the fraction of trajectories in which the reactants, having passed through the TS, reverse direction and start moving apart, before reversing again and forming the product. Only 14−15% of gas phase and SMD trajectories do this, but nearly half (43−46%) of QM/MM and QM/MM+QM trajectories encounter C−C turning points on the product side near the TS (C−C > 1.9 Å). Of these trajectories, the ratio of C_1C_2 to C_3C_4 turning points (Figure 5 numbering) is 90:10 for the QM/MM methods but 60:40 for gas phase and SMD. Both the large fraction of QM/MM turning points, and the
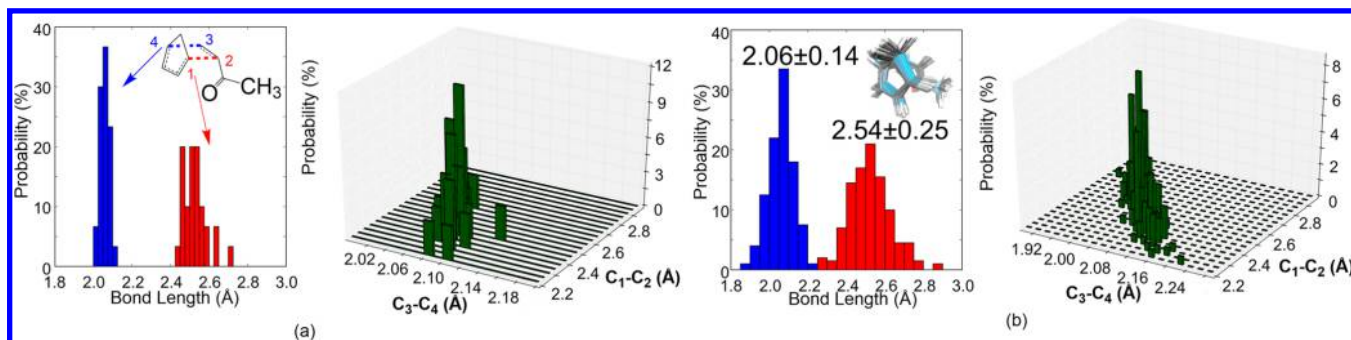

Figure 2. (a) Distribution of forming bond lengths of 20 SPTSs of the endo Diels−Alder reaction between CP and MVK according to step 4. Forming bonds are shown as blue and red dotted lines on the figure. (b) Transition zones for the forming bonds, i.e., the most probable 98% of the distribution of forming bond lengths of 200 sampled transition states according to step 5. Inset: 200 superimposed sampled structures.
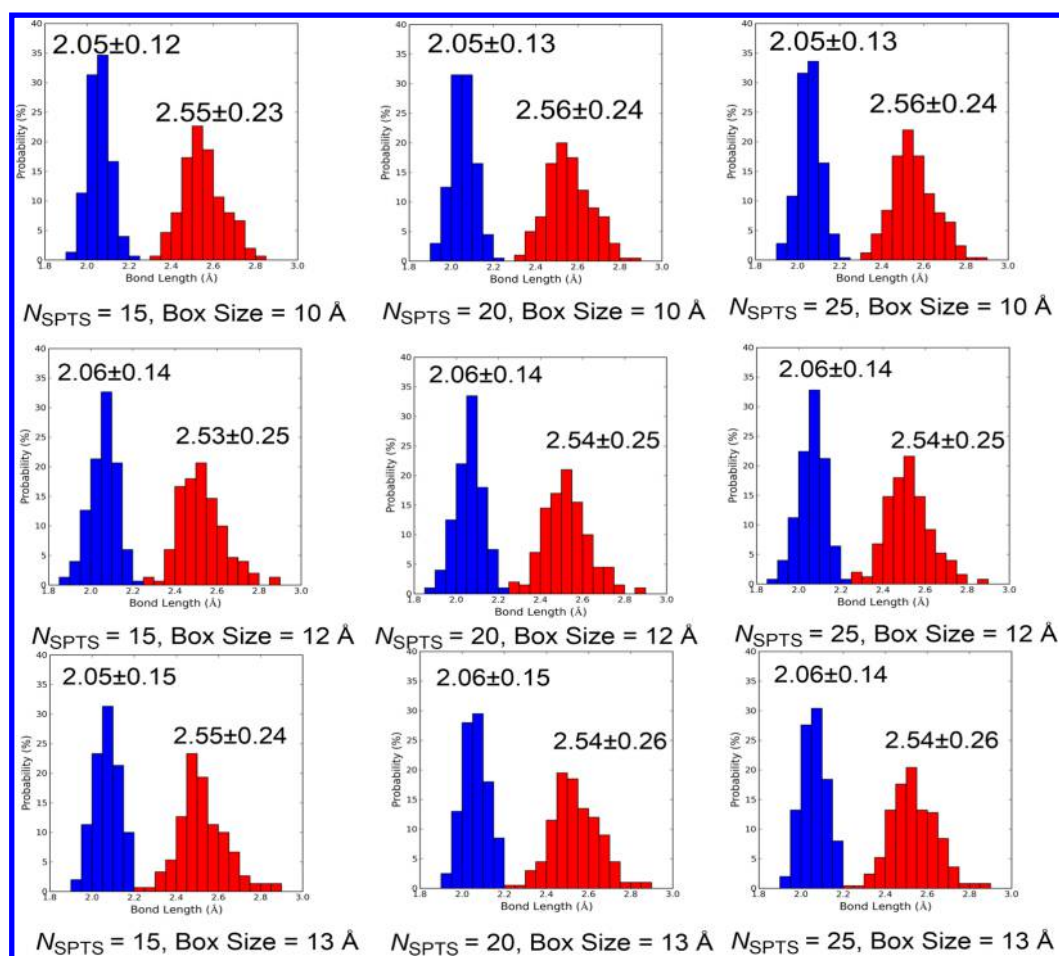
Figure 3. Test for statistical convergence. Protocol steps 2−5 are carried out with box sizes of 10, 12, and 13 Å and N_{SPTS} = 15, 20, 25; transition zones are plotted for each combination. Statistical convergence occurs with a 12 Å box and N_{SPTS} = 20.
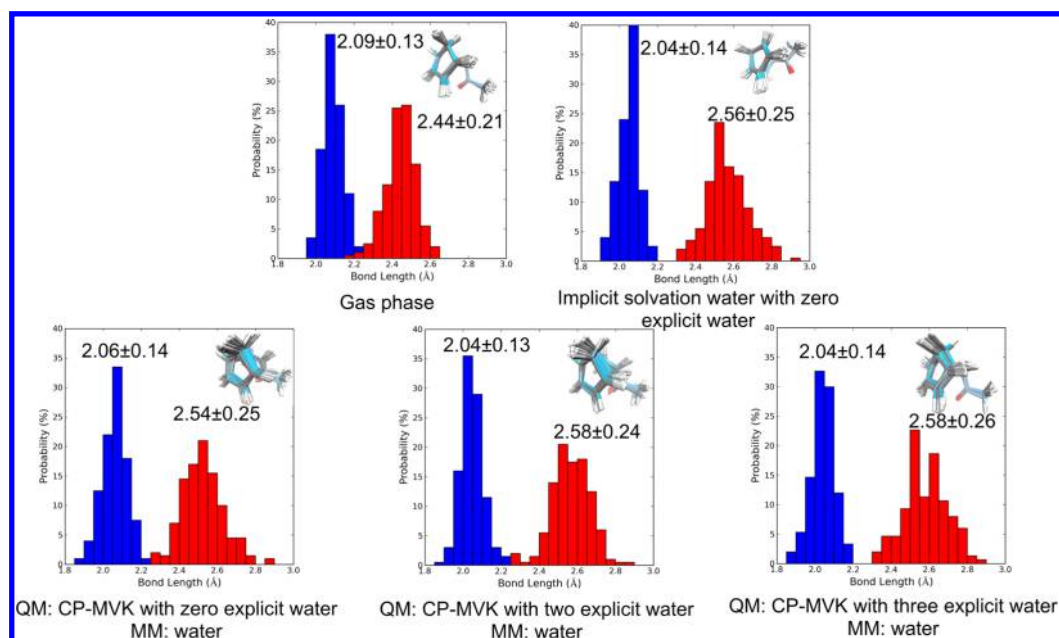

Figure 4. Transition zones of the endo-CP-MVK reaction at 300 K in the gas phase, with SMD implicit water solvation and with explicit water (12 Å box, N_{SPTS} = 20). Insets at the upper right show 200 superimposed sampled structures.

strong preference of the QM/MM methods for the zwitterionic stabilization[42] afforded by large amplitude C_1C_2 motion,

indicate a substantive change in the computed dynamics in explicit solvent compared to implicit solvent. In this reaction,
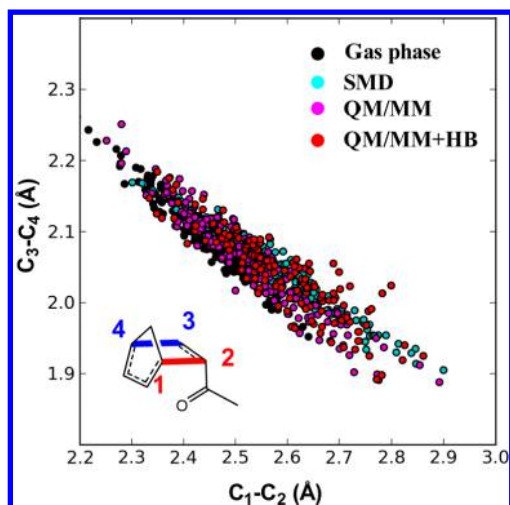
Figure 5. C−C bond lengths for sampled TS points in gas phase, SMD, QM/MM and QM/MM+QM. A total of 150 points are plotted for each.

Table 1. Time Gaps (fs) for Bond Formation and the Percent of Time Gaps >35 fs[a]

	gas phase	SMD	QM/MM	
			0 QM[b]	3 QM[b]
mean gap ± σ[c]	11 ± 6	17 ± 11	20 ± 11	25 ± 14
maximum gap	27	86	82	88
percent >35 fs	0	5	9	19

[a]Vibrational period of a C−C single bond is 30−40 fs. [b]Number of QM water molecules as described in text. [c]Std dev.

which has a steep drop in energy from TS to drop in energy from TS to product, complex motion on the product side of the TS lengthens the time gap but does not affect the exo/endo product ratio. The time gaps of more than 90% of trajectories are within the lifetime of a transition state (60 fs),[43] indicating that the reaction proceeds in a dynamically concerted fashion.

Because Jorgensen's results imply that preferential H-bonding in the TS accounts for the lower barrier in water,[33] we analyzed the H-bond lengths and angles in the QM/MM +QM results. Figure 6a gives the distribution of H-bond lengths in the reactant region (−150 fs), the TS (0 fs), and product region (+150 fs). The mean H-bond length at the TSs is 1.88 Å, which is substantially shorter than reactants (2.02 Å) and products (2.03 Å). The value of 1.88 Å at the TS is close to the 1.9 Å H-bond length reported by Jorgensen, obtained from the O(carbonyl)−H(water) pair distribution function at the TS.[33c] The distribution of H-bond lengths at the TS is narrower than that at the reactant and at the product. Figure 6b shows the distribution of H-bond angle (O(carbonyl)−H(water)−O-(water)) in the reactant, the TS, and the product.[44] The mean value of 158° at the TS is about 10° higher than that at the reactant and at the product. The distribution of H-bond angle at the TS is narrower than that at the reactant and at the product. These results indicate the enhancement of H-bonding during the reaction. (The H-bond analysis of QM/MM results is given in the Figure S3.)

In 14% of trajectories, the O(carbonyl)−H(water)−O-(water) angle rotates by more than 30° from the reactant to the TS (Figure S4). Inspection of these trajectories revealed that the formation of H-bonds in the TS occurs by
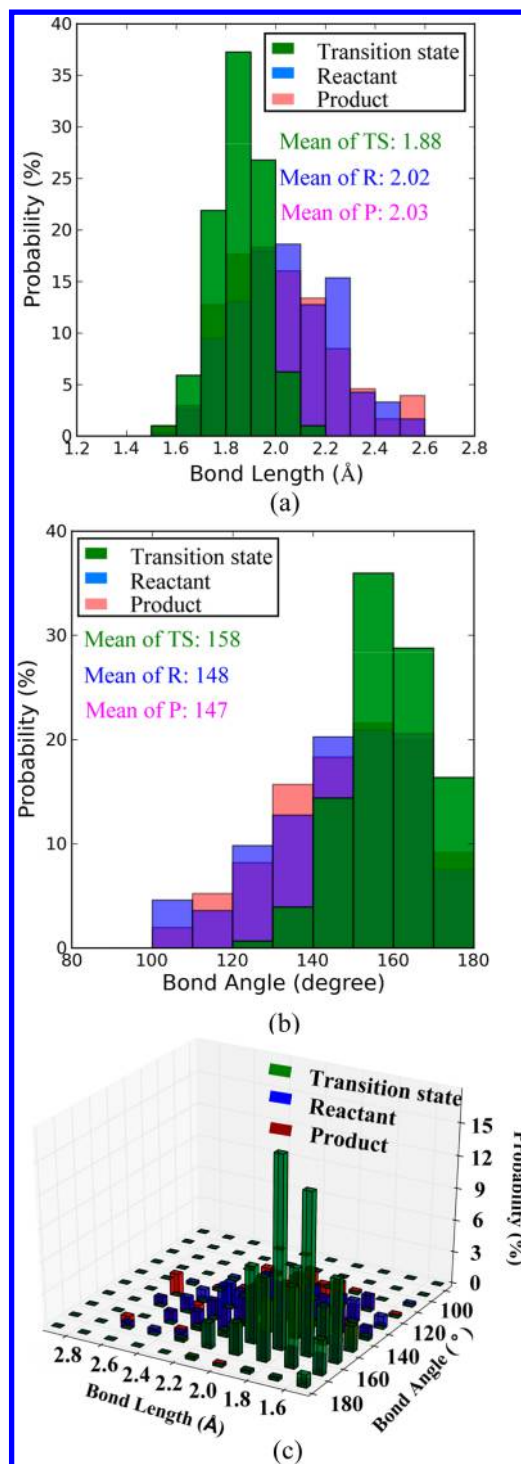

Figure 6. Distribution of (a) hydrogen bonding length (O(carbonyl)−H(water) distance) and (b) hydrogen bonding angle (O(carbonyl)−H(water)−O(water) angle) in transition states (in green, at 0 fs), reactants (in blue, at −150 fs), and products (in pink, at 150 fs). A total of 150 reactive trajectories are used for the analysis. (c) 3D representation of distribution of hydrogen bonding length and angle in the transition states, reactants and products.

reorientation of a neighboring water molecule during the reaction. Figure 7 shows an example. In the upper left frame, at −150 fs, MVK has one strong H-bond (1.93 Å) to water A. The neighboring water molecule B is situated such that an H atom is 3.12 Å away from the carbonyl oxygen of MVK. B then
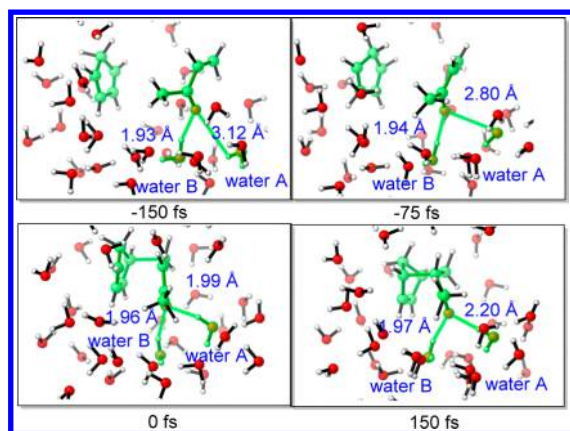
Figure 7. Snapshots taken at −150, −75, 0, and +150 fs of a typical trajectory with three water molecules added into the QM region.

reorients itself toward the oxygen of MVK as the reaction progresses. At −75 fs, the H−O distance is 2.80 Å, and at 0 fs it becomes 1.99 Å, indicating the formation of a second strong hydrogen bond. In the product region at 150 fs, the lengths of the A and B H-bonds are 1.97 and 2.20 Å, respectively. The reorientation of water over a 75 fs time scale illustrates a potent mechanism for preferential stabilization of the TS.

CONCLUSION

We propose a solvent-perturbed transition state (SPTS) sampling scheme as a new QM/MM protocol for solution-phase direct dynamics simulation of chemical reactions. This protocol includes the effect of solvent configuration on the potential energy surface of the reacting system, and allows initial conditions for the reacting system to be sampled quasiclassically by TS normal mode sampling. As a proof of concept, we applied the SPTS scheme to the dynamics of water-accelerated Diels−Alder reaction of cyclopentadiene (CP) and methyl vinyl ketone (MVK). Statistical convergence of the sampling is conveniently monitored by computing the transition zone as a function of the number SPTSs and solvent box size. Mean time gaps between formation of C−C bonds vary from 11 fs for the gas phase to 25 fs for QM/MM+QM, with tails of the distributions up to >80 fs. Nearly half of QM/MM and QM/MM+QM trajectories encounter C−C turning points on the product side of the TS. This complex motion lengthens the time gap but does not affect the exo/endo product ratio. The time gaps of more than 90% of trajectories are within the lifetime of the transition state (60 fs), indicating that the reaction proceeds in a dynamically concerted fashion. In QM/MM+QM trajectories, the mean O(carbonyl)−H-(water) distance of H-bonds at the TS is 0.14 Å shorter than in the MVK reactant, and the mean O(carbonyl)−H(water)−O(water) angle of H-bonds at the TS is 10° larger than in the MVK reactant. In 14% of these trajectories, the formation of H-bonds in the TS occurs by reorientation of a water molecule during the reaction. These results support the conclusion of Jorgensen and co-workers[33] that preferential H-bond stabilization in the TS makes the largest contribution to water acceleration of Diels−Alder reactions.

ASSOCIATED CONTENT

Ⓢ Supporting Information

The Supporting Information is available free of charge on the ACS Publications website at DOI: 10.1021/acs.jctc.5b01029.

Computational procedures and scripts, coordinates and energies of gas phase and SMD stationary points, transition vectors and imaginary frequencies of 20 SPTSs, cubic water packing diagram, Mulliken charges, distributions of H bonding length and H bonding angle, distribution of angle difference, populations of C−C bond lengths vs time (PDF)

Movie of Figure 7 (MP4)

AUTHOR INFORMATION

Corresponding Authors
*C. Doubleday. E-mail: ced3@columbia.edu.
*K. N. Houk. E-mail: houk@chem.ucla.edu.

Notes
The authors declare no competing financial interest.

REFERENCES

(1) (a) Newman-Evans, R. H.; Carpenter, B. K. *J. Am. Chem. Soc.* **1984**, *106*, 7994−7995. (b) Carpenter, B. K. *J. Am. Chem. Soc.* **1985**, *107*, 5730−5732. (c) Newman-Evans, R. H.; Simon, R. J.; Carpenter, B. K. *J. Org. Chem.* **1990**, *55*, 695−711. (d) Carpenter, B. K. *Acc. Chem. Res.* **1992**, *25*, 520−528.

(2) (a) Lourderaj, U.; Hase, W. L. *J. Phys. Chem. A* **2009**, *113*, 2236−2253. (b) Lourderaj, U.; Park, K.; Hase, W. L. *Int. Rev. Phys. Chem.* **2008**, *27*, 361−403.

(3) (a) Carpenter, B. K. *Chem. Rev.* **2013**, *113*, 7265−7286. (b) Carpenter, B. K. *Annu. Rev. Phys. Chem.* **2005**, *56*, 57−89. (c) Carpenter, B. K. In *Reactive Intermediate Chemistry*, Moss, R. A., Platz, M. A., Jones, M., Jr., Eds.; Wiley: Hoboken, NJ, 2004; pp 925−960. (d) Carpenter, B. K. *J. Phys. Org. Chem.* **2003**, *16*, 858−868.

(4) Rehbein, J.; Carpenter, B. K. *Phys. Chem. Chem. Phys.* **2011**, *13*, 20906−20922.

(5) Yamataka, H. *Adv. Phys. Org. Chem.* **2010**, *44*, 173−222.

(6) Sun, L. P.; Song, K. Y.; Hase, W. L. *Science* **2002**, *296*, 875−878.

(7) Sun, R; Park, K.; de Jong, W. A.; Lischka, H.; Windus, T. L.; Hase, W. L. *J. Chem. Phys.* **2012**, *137*, 044305.

(8) (a) Ammal, S. C.; Yamataka, H.; Aida, M.; Dupuis, M. *Science* **2003**, *299*, 1555−1556. (b) Yamataka, H.; Aida, M.; Dupuis, M. *J. Phys. Org. Chem.* **2003**, *16*, 475. (c) Yamataka, H.; Aida, M.; Dupuis, M. *Chem. Phys. Lett.* **2002**, *353*, 310. (d) Yamataka, H.; Aida, M.; Dupuis, M. *Chem. Phys. Lett.* **1999**, *300*, 583−587.

(9) (a) Bekele, T.; Christian, C. F.; Lipton, M. A.; Singleton, D. A. *J. Am. Chem. Soc.* **2005**, *127* (25), 9216−9223. (b) Ussing, B. R.; Hang, C.; Singleton, D. A. *J. Am. Chem. Soc.* **2006**, *128*, 7594−7607.

(10) Bach, A.; Hostettler, J. M.; Chen, P. *J. Chem. Phys.* **2006**, *125*, 024304.

(11) Litovitz, A. E.; Keresztes, I.; Carpenter, B. K. *J. Am. Chem. Soc.* **2008**, *130*, 12085−12094.

(12) Glowacki, D. R.; Marsden, S. P.; Pilling, M. J. *J. Am. Chem. Soc.* **2009**, *131*, 13896−13897.

(13) Zheng, J.; Papajak, E.; Truhlar, D. G. *J. Am. Chem. Soc.* **2009**, *131*, 15754−15760.

(14) Glowacki, D. R.; Liang, C. H.; Marsden, S. P.; Harvey, J. N.; Pilling, M. J. *J. Am. Chem. Soc.* **2010**, *132*, 13621−13623.

(15) Zhang, X. H.; Zummack, W.; Schroder, D.; Weinhold, F. A.; Schwarz, H. *Chem. - Eur. J.* **2009**, *15*, 11815−11819.

(16) McKee, M. L.; Reisenauer, H. P.; Schreiner, P. R. *J. Phys. Chem. A* **2014**, *118*, 2801−2809.

(17) (a) Ezra, G. S.; Waalkens, H.; Wiggins, S. *J. Chem. Phys.* **2009**, *130*, 164118. (b) Collins, P.; Carpenter, B. K.; Ezra, G. S.; Wiggins, S. *J. Chem. Phys.* **2013**, *139*, 154108. (c) Collins, P.; Kramer, Z. C.; Carpenter, B. K.; Ezra, G. S.; Wiggins, S. *J. Chem. Phys.* **2014**, *141*, 034111.

(18) (a) Merrer, D. C.; Rablen, P. R. *J. Org. Chem.* **2005**, *70*, 1630−1635. (b) Rablen, P. R.; Paiz, A. A.; Thuronyi, B. W.; Jones, M. *J. Org. Chem.* **2009**, *74*, 4252−4261.

(19) Zhou, J.; Schlegel, H. B. *J. Phys. Chem. A* **2009**, *113*, 1453−1458.

(20) (a) Schmittel, M.; Vavilala, C.; Jaquet, R. *Angew. Chem., Int. Ed.* **2007**, *46*, 6911−6914. (b) Samanta, D.; Rana, A.; Schmittel, M. *J. Org. Chem.* **2014**, *79*, 2368−2376. (c) Samanta, D.; Rana, A.; Schmittel, M. *J. Org. Chem.* **2014**, *79*, 8435−8439.

(21) Biswas, B.; Collins, S. C.; Singleton, D. A. *J. Am. Chem. Soc.* **2014**, *136*, 3740−3743.

(22) (a) Siebert, M. R.; Zhang, J. X.; Addepalli, S. V.; Tantillo, D. J.; Hase, W. L. *J. Am. Chem. Soc.* **2011**, *133*, 8335−8343. (b) Siebert, M. R.; Manikandan, P.; Sun, R.; Tantillo, D. J.; Hase, W. L. *J. Chem. Theory Comput.* **2012**, *8*, 1212−1222.

(23) (a) Pemberton, R. P.; Hong, Y. J.; Tantillo, D. J. *Pure Appl. Chem.* **2013**, *85*, 1949−1957. (b) Hong, Y. J.; Tantillo, D. J. *Nat. Chem.* **2014**, *6*, 104−111. (c) Pemberton, R. P.; Tantillo, D. J. *Chemical Science* **2014**, *5*, 3301−3308.

(24) (a) Carpenter, B. K. *J. Am. Chem. Soc.* **1995**, *117*, 6336−6344. (b) Hrovat, D. A.; Fang, S.; Borden, W. T.; Carpenter, B. K. *J. Am. Chem. Soc.* **1997**, *119*, 5253−5254. (c) Nummela, J. A.; Carpenter, B. K. *J. Am. Chem. Soc.* **2002**, *124*, 8512−8513.

(25) (a) Doubleday, C.; Bolton, K.; Hase, W. L. *J. Am. Chem. Soc.* **1997**, *119*, 5251−5252. (b) Doubleday, C. *J. Phys. Chem. A* **2001**, *105*, 6333−6341. (c) Doubleday, C.; Suhrada, C. P.; Houk, K. N. *J. Am. Chem. Soc.* **2006**, *128*, 90−94.

(26) (a) Chen, Z.; Nieves-Quinones, Y.; Waas, J. R.; Singleton, D. A. *J. Am. Chem. Soc.* **2014**, *136*, 13122−13125. (b) Glowacki, D. R.; Orr-Ewing, A. J.; Harvey, J. N. *J. Chem. Phys.* **2011**, *134*, 214508. (c) Sato, M.; Yamataka, H.; Komeiji, Y.; Mochizuki, Y.; Ishikawa, T.; Nakano, T. *J. Am. Chem. Soc.* **2008**, *130*, 2396−2397. (d) Ruiz-Pernía, J. J.; Tuñón, I.; Moliner, V.; Hynes, J. T.; Roca, M. *J. Am. Chem. Soc.* **2008**, *130*, 7477−7488. (e) Mann, D. J.; Halls, M. D. *Phys. Chem. Chem. Phys.* **2002**, *4*, 5066−5071. (f) Bolton, K.; Hase, W. L.; Doubleday, C. *J. Phys. Chem. B* **1999**, *103*, 3691−3698.

(27) Case, D. A.; et al. *AMBER 14*; University of California: San Francisco, 2014.

(28) Frisch, M. J.; et al. *Gaussian 09*, Revision D.01; Gaussian Inc.: Wallingford, CT, 2013.

(29) (a) Alhambra, C.; Gao, J. L.; Corchado, J. C.; Villa, J.; Truhlar, D. G. *J. Am. Chem. Soc.* **1999**, *121*, 2253−2258. (b) Alhambra, C.; Corchado, J. C.; Sanchez, M. L.; Gao, J. L.; Truhlar, D. G. *J. Am. Chem. Soc.* **2000**, *122*, 8197−8203. (c) Alhambra, C.; Corchado, J.; Sanchez, M. L.; Garcia-Viloca, M.; Gao, J.; Truhlar, D. G. *J. Phys. Chem. B* **2001**, *105*, 11326−11340. (d) Truhlar, D. G.; Gao, J. L.; Garcia-Viloca, M.; Alhambra, C.; Corchado, J.; Sanchez, M. L.; Poulsen, T. D. *Int. J. Quantum Chem.* **2004**, *100*, 1136−1152.

(30) Peslherbe, G. H.; Wang, H. B.; Hase, W. L. *Adv. Chem. Phys.* **1999**, *105*, 171−201.

(31) (a) Garcia-Viloca, M.; Alhambra, C.; Truhlar, D. G.; Gao, J. L. *J. Comput. Chem.* **2003**, *24*, 177−190. (b) Poulsen, T. D.; Garcia-Viloca, M.; Gao, J. L.; Truhlar, D. G. *J. Phys. Chem. B* **2003**, *107*, 9567−9578. (c) Tejero, I.; Garcia-Viloca, M.; Gonzalez-Lafont, A.; Lluch, J. M.; York, D. M. *J. Phys. Chem. B* **2006**, *110*, 24708−24719. (d) Kanaan, N.; Ferrer, S.; Marti, S.; Garcia-Viloca, M.; Kohen, A.; Moliner, V. *J. Am. Chem. Soc.* **2011**, *133*, 6692−6702.

(32) (a) Rideout, D. C.; Breslow, R. *J. Am. Chem. Soc.* **1980**, *102*, 7816. (b) Breslow, R.; Guo, T. *J. Am. Chem. Soc.* **1988**, *110*, 5613. (c) Breslow, R. *Acc. Chem. Res.* **1991**, *24*, 159−164.

(33) (a) Blake, J. F.; Lim, D.; Jorgensen, W. L. *J. Org. Chem.* **1994**, *59*, 803−805. (b) Chandrasekhar, J.; Shariffskul, S.; Jorgensen, W. J. *J. Phys. Chem. B* **2002**, *106*, 8078−8085. (c) Acevedo, O.; Jorgensen, W. L. *J. Chem. Theory Comput.* **2007**, *3*, 1412−1419.

(34) Jorgensen, W. L.; Chandrasekhar, J.; Madura, J. D.; Impey, R. W.; Klein, M. L. *J. Chem. Phys.* **1983**, *79*, 926−935.

(35) Marenich, A. V.; Cramer, C. J.; Truhlar, D. G. *J. Phys. Chem. B* **2009**, *113*, 6378−6396.

(36) In the general case, step 2 would be preceded by a search for the TS region, which typically involves umbrella sampling to compute the potential of mean force along a reaction coordinate to find the region of highest free energy. We currently assume that the TS region is close to the saddle point determined in step 1.

(37) Use of the gas phase saddle point in place of TS_w in steps 2−6 made a negligible difference in the final results for this test case. In general, however, a transition structure computed with implicit solvation is expected to be the better zero-order choice and we use TS_w in the subsequent description.

(38) (a) Dapprich, S.; Komáromi, I.; Byun, K. S.; Morokuma, K.; Frisch, M. J. *J. Mol. Struct.: THEOCHEM* **1999**, *462*, 1−21. (b) Vreven, T.; Byun, K. S.; Komáromi, I.; Dapprich, S.; Montgomery, J. A., Jr.; Morokuma, K.; Frisch, M. J. *J. Chem. Theory Comput.* **2006**, *2*, 815−26.

(39) Hase, W. L.; Duchovic, R. J.; Hu, X.; Lim, K.; Lu, D.-h.; Peslherbe, G. H.; Swamy, K. N.; VandeLinde, S. R.; Wang, H.; Wolfe, R. J. "VENUS 96, a General Chemical Dynamics Computer Program", QCPE671.

(40) SPTS saddle points have $3N_1 − 1$ vibrational frequencies instead of $3N_1 − 7$ as in the gas phase. Translational and rotational motions of the solute are transformed into vibrational motions by interaction with surrounding solvent molecules.

(41) After 150 fs propagation in the product direction, the forming C−C bond lengths are <1.59 Å in all reactive trajectories. In the reactant direction, both C−C bonds are >3.5 Å after 150 fs.

(42) Mulliken charge distribution of reactant, TS and endo product are shown in Figure S2 to support the zwitterionic character of the TS.

(43) (a) Eyring, H. *Trans. Faraday Soc.* **1938**, *34*, 41−48. (b) Black, K.; Liu, P.; Xu, L.; Doubleday, C.; Houk, K. N. *Proc. Natl. Acad. Sci. U. S. A.* **2012**, *109*, 12860−12865.

(44) The water molecules that form an H-bond with the MVK are located by the criteria: (1) O(carbonyl)−O(water) distance is within 3.0 Å, (2) O(carbonyl)−H(water) is within 2.6 Å, and (3) O(carbonyl)−H(water)−O(water) is higher than 180°.